Electron emission from water vapor under the impact of 250-keV protons

Abhijeet Bhogale [1], S. Bhattacharjee,[1] M. Roy Chowdhury,[1] Chandan Bagdia [1], M. F. Rojas,[2] J. M. Monti,[2] A. Jorge,[3]
M. Horbatsch [4], T. Kirchner [4], R. D. Rivarola,[2] and L. C. Tribedi [1,*]

[1]*Tata Institute of Fundamental Research, Homi Bhabha Road, Colaba, Mumbai 400005, India*
[2]*Instituto de Fisica Rosario (CONICET-UNR), Universidad Nacional de Rosario, 2000 Rosario, Argentina*
[3]*Departamento de Química, Universidad Autónoma de Madrid, Cantoblanco, E-28049 Madrid, Spain*
[4]*Department of Physics and Astronomy, York University, Toronto, Ontario, Canada M3J 1P3*

Absolute double differential cross sections (DDCS) of low-energy electron emission from water molecule were measured upon collisions with 250-keV protons for emission angles between 30–150 degrees. The electrons having energies between 1 and 600 eV were detected by using hemispherical electrostatic analyzer. The single differential (SDCS) and total cross section (TCS) were calculated by integrating the DDCS and SDCS, respectively. The measured DDCS, SDCS, and TCS were compared with the classical trajectory Monte Carlo (CTMC) model, using a dynamical approach in which a time-dependent screening is considered. The continuum-distorted-wave eikonal-initial state (CDW-EIS) theoretical model has also been used to explain the energy and angular distribution data. The angular distribution of the DDCS are very well reproduced by the CTMC approach. The TCS calculated by the CTMC model matches better with the measured values as compared to the CDW-EIS estimation. The forward-backward angular asymmetry parameter was also estimated to test the validity of the state-of-the-art theoretical models used. Finally the recently developed CDW-EIS calculations considering a residual target dynamic charge (DC-CDW-EIS) is shown to provide an improved agreement with the experiments compared to the CDW-EIS. The present data and interpretation should provide inputs towards energy loss calculations required for the radiobiology involved in the hadron therapy of cancer.

I. INTRODUCTION

There have been several studies on the measurement of double differential cross sections (DDCS) for emitted electrons from gaseous targets impacted by protons with different energies. The experimental study of ionization of molecules by fast ions have been an important topic in general atomic and molecular collision physics. These studies have provided crucial inputs towards the development of various quantum mechanical theoretical models. The interpretation of the experimental data in terms of the models depends on the various inputs used or assumptions made in the theory regarding the interaction potential and the molecular structures, etc. The energy and charge state of the projectile ions are the most crucial parameters to indicate the validity of the theoretical models. Water can be considered as benchmark for many small molecules, such as many diatomic or triatomic molecules. Understanding the ionization of the water molecule in terms of the theoretical models will be a step forward to explore the ionization dynamics for even larger molecules. The continuum-distorted-wave eikonal-initial state (CDW-EIS) model has recently been upgraded by inclusion of a time-dependent charge and the classical trajectory Monte Carlo (CTMC) model has also been improved by the inclusion of a dynamic screening. It is important to test the valid-

ity of these newly developed state-of-the-art models under stringent collision conditions, i.e., at relatively low-energy ions.

The studies on electron emission from water and other biomolecules (such as nucleobases, etc.) are quite important for radiobiology, particularly, in connection with the hadron therapy [1] of cancer [2] and damage of living cells by cosmic-ray ions during human space missions [3]. In biomedical applications, such as radiobiology of cancer therapy using high-energy protons, the cross sections of low-energy electrons become an important tool [4]. In such applications, the studies on the water molecules gain first importance because of their high abundance in all biological systems. Toburen *et al.* have measured absolute cross sections for emitted electrons from water molecules by collision with protons of energies from 0.3–1.5 MeV [5]. They have compared the cross sections of water and oxygen molecules as per their weakly bound electrons.

Ionization cross sections have been reported for electrons emitted in collisions between neutral hydrogen atoms of energy 20–150 keV and water vapor [6,7]. Similar studies have been reported for proton projectiles with energies 1 MeV [8], 0.3–1.5 MeV [5], 0.3–2 MeV [9], 4 MeV/u [10] colliding with water molecules. Electronic stopping cross sections have also been studied theoretically [11–13], as well as experimentally [14,15] for water molecules impacted by protons.

In this paper, we report differential ionization cross sections of H_2O under the impact of a 250-keV proton

---

*lokesh@tifr.res.in; ltribedi@gmail.com

beam. Electrons ejected from the target have been analyzed in order to obtain the electron double differential cross section (e-DDCS), single differential cross section (SDCS), and the total cross section (TCS). Experimental data have been supported by the theoretical models based on the new CTMC calculations, CDW-EIS approach [10,16,17], and CDW-EIS calculations considering a residual target dynamic charge (DC-CDW-EIS).

Recently the modified version of the CTMC model [18,19] has been applied to ion collisions with water molecules at higher energy. This was a dynamical approach in which a time-dependent screening was used to consider the change in charge state after removal of an electron. This dynamical model has been tested for water [18] for the energy range of $0.47 \leqslant Z_p/v_p \leqslant 1.03$ by comparing the experimental data for C^{6+} [10], O^{8+} [17,20], and Si^{13+} [10] projectiles. Determining its validity for projectiles in various energy regimes becomes important. In this work the same CTMC model has been applied. Therefore, the model will be validated for low Z_p/v_p, i.e., 0.146, with 250-keV proton projectile collisions with water molecules.

In this model a three-center potential is considered to account for the three nuclear charges and passive electrons. Along with that a time-dependent charge-state target potential is also introduced [18]. The nuclear motion is approximated by a semiclassical treatment and then electron motion is approximated by classical statistical mechanics. In a previous model, the same potential was introduced for the system of a frozen H_2O^+ core with active electrons, which accurately predicted the total cross sections [21,22].

The CDW-EIS model is known to produce a reasonable agreement with experimental data for a wide variety of collision systems involving bare ions as projectiles, and atomic and molecular targets with collision energies from intermediate to high. In this model, to evaluate single ionization from bare-ion impact, within the independent electron model, a multielectronic system can be reduced to a monoelectronic one [23]. The nonionized electrons are considered frozen during the collision process. In the entry channel the projectile distortion is chosen to represent the asymptotic Coulombic behavior of projectile active-electron interaction represented by an eikonal phase, and as a Coulomb continuum function in the exit channel. In the post version of the CDW-EIS model, the interaction between the active electron and the residual target is usually considered to be purely Coulombic. In this approximation, the effect of the dynamic screening due to the interaction between the residual target and the active electron is partially neglected. In this way, the prior version of the CDW-EIS contains more physical information as the radial correlation between the active and passive electrons is considered through the initial target bound orbitals [24]. In this work the initial molecular orbitals are described by the complete neglect of differential orbitals (CNDO) approximation in which every molecular orbital is considered as a linear combination of atomic orbitals of the atomic constituents of the molecule. The detailed description of the CDW-EIS calculations has already been published [16] and compared with the experimental data for high-energy projectiles on water target [10,17,20].

II. EXPERIMENTAL DETAILS AND MEASUREMENTS

A. ECR ion source and accelerator

The present work is carried out using an ECR ion source connected to a 400-kV accelerator in TIFR Mumbai. In the ion source, initially, plasma was created in the plasma chamber using hydrogen gas and then the proton beam was extracted by applying a 30-kV extraction potential. In a later stage, it was then accelerated up to 250 keV and tuned up to scattering chamber by using Einzel lens, analyzing magnet, quadrupole triplet with X-Y deflectors, switching magnet, pair of four-jaw slits and collimators. Beam-line vacuum was maintained to 5×10^{-9} mbar.

The experiments were performed in the high vacuum scattering chamber, which is kept at the end of the 50° south beam line. The base vacuum was 5×10^{-7} mbar. During the experiment, the chamber was flooded with the gas of interest at about 10^{-5} mbar. A differentially pumped chamber with collimators was used to maintain the beam-line vacuum. The broad beam was cut by using an extended collimator of diameter 2 mm at entrance and 4 mm at the exit. The inner side of the chamber is covered with two μ-metal sheets to reduce Earth's magnetic field to about $\sim$5–10 mG, which enables us to detect low-energy electrons during an experiment.

The hemispherical electron energy analyzer was kept on a rotating table mounted at the base of the scattering chamber. This has been explained earlier in a schematic diagram [25,26]. At the exit of the hemispherical analyzer, a channel electron multiplier (CEM) has been installed to count electrons of particular energy selected. The front plate of the CEM was biased with $+100$ V to enhance the collection efficiency of low-energy electrons up to a certain uniform efficiency level. The entrance and exit slits were biased with pre-acceleration voltage $+6$ V to increase the detection efficiency of low-energy electrons. The energy resolution of the spectrometer is 6% of the energy selected. The total absolute error in the measured e-DDCS was within 15–19 %. The electron spectrometer can be rotated around the interaction region, from 20°–90° in forward angles and 90°–160° in backward angles.

The scattering chamber was flooded with water vapor with a pressure of 0.1 mTorr, which was controlled by the solenoid valve and MKS Baratron manometer. For gaseous water target, millipore water was stored in the stainless steel container, which was then connected to the chamber using stainless steel tubings. Water gets self-evaporated due to its low vapor pressure, i.e., 27 mTorr, The electrons were detected and counted for the energy range of 1–600 eV at various angles of 30°, 45°, 60°, 75°, 90°, 105°, 120°, 135°, 150°.

The data acquisition was accomplished by using a LABVIEW program developed in house. During the experiments, electron energies are selected by setting appropriate spectrometer voltages through the LABVIEW card. The signal generated in the CEM was processed in timing filter amplifier (TFA), constant fraction discriminator (CFD), and level translator, which is later fed into the DAQ system comprising of the LABVIEW software and National Instruments (NI) card where it is recorded as electron counts. Simultaneously, current integrated (CI) pulses are also fed into the program

to get projectile counts. In the end, electron energy, CI, and electron counts are recorded in the computer program as raw data. Background data was also collected similarly by closing the gas inlet valve on the chamber. A sufficient number of projectiles have been set initially to get better statistics in electron counting for a particular energy range of electrons. During each data set, it was ensured that the pressure is stable to minimize the error in the number density of molecules.

III. CTMC MODEL

Within the CTMC method, the quantum description of the electron dynamics is approximated by a classical statistical ensemble. For each molecular orbital (MO), a microcanonical ensemble is built with the corresponding MO ionization energy, and every initial ensemble contains 1×10^5 trajectories. The statistical distribution interacts with the water cation through a multicenter potential [21] to account for the two hydrogen and the oxygen atoms, which are assumed to remain in the ground-state geometric arrangement. The screening charges in the potential are $N_O = 7.185$ and $N_H = (9 - N_O)/2$. The projectile interaction is given by a Coulomb potential. In order to study the influence of the dynamical response due to the ionization processes in the target, we introduce dynamical screening charges [18] by making the parameters $N_O = N_O(t)$ and $N_H = N_H(t)$ dependent on the net electron removal from the target, $P_{\text{Net}}^{\text{Removal}}(t)$. During the collision dynamics, the time evolution is monitored in small time steps ($\Delta t = 0.05$ a.u.) in the region where the collision happens so that the time-dependent target potentials are updated on a fine time grid. The dependence in time is done so that for $P_{\text{Net}}^{\text{Removal}} > 1$ $N_O(t)$ and $N_H(t)$ decrease linearly up to the limit when $P_{\text{Net}}^{\text{Removal}} = 10$, when the two screening charges get to 0 and the remaining potentials at each center are Coulombic. When the collision is finished, the single-electron probabilities for each MO labeled by j are calculated as $p_j^i = n_j^i/n_{j,\text{Tot}}$, where $i = \text{cap, ion}$ stands for ionization and electron capture, respectively, $n_{j,\text{Tot}} = 10^5$ is the total number of initial trajectories, and n_j^i is the number of trajectories, which end the collision in each inelastic process, calculated using the energy criterion described in Ref. [18]. In order to determine the doubly and singly differential cross sections, DDCS and SDCS, respectively, we define boxes for both ΔE_{el} and $\Delta \Omega_{\text{el}}$ in which the ionized electrons are binned. The probabilities are then

$$\frac{d^2 P}{dE_{\text{el}} d\Omega_{\text{el}}} = 2 \sum_{j=1}^{5} \frac{n_j^k}{n_{j,\text{Tot}} \Delta E_{\text{el}} \Delta \Omega_{\text{el}}} \, , \quad (1)$$

where n_j^k is the number of ionized electrons for each ΔE_{el} and $\Delta \Omega_{\text{el}}$ and the factor of two accounts for the fact that each MO is occupied by two electrons due to spin degeneracy. The sizes of the boxes ΔE_{el} and $\Delta \Omega_{\text{el}}$ are adapted to the experimental values.

IV. CDW-EIS MODEL

The well-known distorted wave theory CDW-EIS (continuum distorted wave-eikonal initial state) in its prior version was also used to calculate the ionization cross sections. In

the CDW-EIS approximation for single ionization under the impact of a bare ion, a multielectronic target is usually reduced to a monoelectronic one, assuming that the rest of the electrons remain frozen in their initial orbitals. The initial wave function of the active electron bound to a particular molecular orbital (MO) is described by means of the CNDO approximation originally developed by Pople *et al.* [27–29]. Then, for the computation of the DDCS, we make use of the method proposed by Senger *et al.* [30]. In this treatment, all the overlapping integrals are neglected and the resulting DDCS for any MO is then reduced to a weighted sum of atomic DDCS corresponding to the atomic constituents of the molecule (see also Ref. [16] and references therein). In the exit channel the continuum of the active electron in the residual target field is approximated by a Coulombic one with an effective charge $\tilde{Z}_T$ usually chosen with Belkic's criteria [31] $\tilde{Z}_{\text{eff}} = \sqrt{-2 n^2 \varepsilon_0}$, being ε_0 the binding energy of a given MO and n the principal quantum number of the atomic orbitals in its linear combination. This choice for the effective charge in the final target continuum state was shown to give overall good qualitative results for single ionization in many collision systems but was proven to show a large underestimation of DDCS in backwards emission for large emission energies (see Ref. [32]).

In order to improve the representation of the residual target continuum state, a dynamic charge depending on the emission angle $\tilde{Z}_{\text{eff}}(\theta)$ was proposed by Rojas *et al.* [33] considering a linear variation taking the charge given by Belkic's criteria for an emission angle $\theta = 0°$, and the target nuclear charge for $\theta = 180°$. This showed a major improvement in the description of backward emission for large enough ejection energies in single ionization of multielectronic targets. Here we also consider this dynamic charge for DDCS CDW-EIS calculations for high enough emission energies (see Ref. [33]).

V. RESULTS AND DISCUSSION

A. Estimation of DDCS of H$_2$O

The absolute DDCS, $d^2\sigma/d\epsilon_e d\Omega_e$, as a function of electron emission energy (ϵ_e) and emission angle (Ω_e), have been obtained by using the equation derived from first principles [6,10,26]. Figure 1 represents the energy distribution of absolute DDCS for six emission angles. Some of the DDCS data are displayed in Table I. The experimental data have been overlapped with the theoretically calculated DDCS using the CTMC, CDW-EIS, and DC-CDW-EIS models. From each spectrum, it can be seen that the DDCS falls off rapidly as the energy of the emitted electrons increases. The low-energy part of the DDCS is due to the soft collision process, i.e., electrons are ejected due to the high impact parameter involving small momentum transfer. The middle part of the DDCS spectrum is due to the slightly lower impact parameter, where the two-center effect plays a major role in which the emitted electrons are influenced by the fields of positively charged target and the outgoing projectile. The high-energy electrons are emitted as an effect of large perturbation during small impact parameter collisions.

From Fig. 1 it is seen that the experimental results show excellent agreement with the CTMC calculations as compared
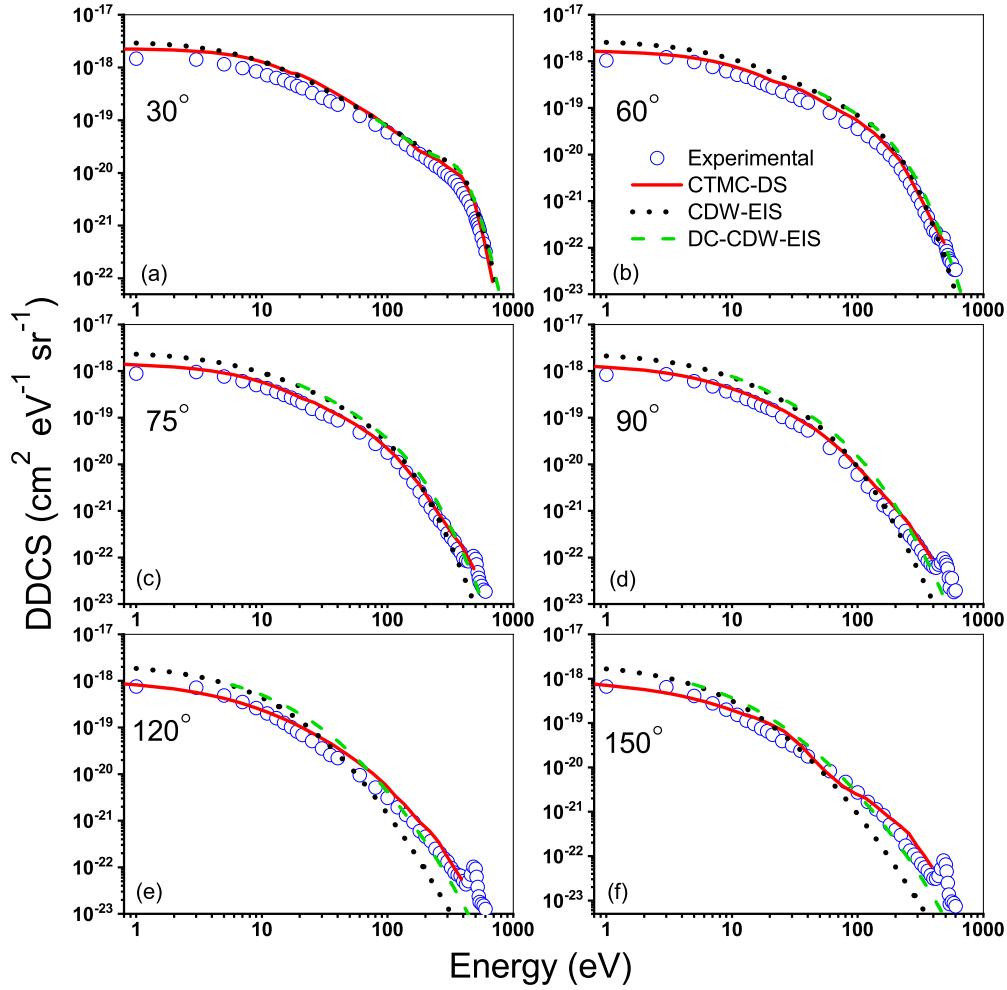
FIG. 1. Absolute electron DDCS shown for six angles along with the CTMC, CDW-EIS, and DC-CDW-EIS calculations.

with the CDW-EIS model calculations. However, CDW-EIS results qualitatively agreed with the experimental data in forward angles but as one goes towards the backward angles, mismatch increases. Nonetheless, it can be seen that, in DC-CDW-EIS, the consideration of an effective charge depending on the emission angle in the residual target continuum state largely improves the backward emission. The idea of the dynamic charge in the DC-CDW-EIS approximation being solely depending on emission angle is only valid for high enough emission energies, given it meant to enhance the backward emission region. Thus, for lower emission energies the usual CDW-EIS with Belkic's charge is employed and DC-CDW-EIS is employed above certain energy, as for example, above 10, 20, or 50 eV, etc. In backward angles, a peak at 480 eV become prominent, which corresponds to the K-LL Auger electron emission from oxygen in H_2O target. The only discrepancy we see in DDCS calculated by the CTMC model is slightly higher values in forward angles in the low-energy range as compared to the experimental data. The comparison between experiment and theory can be better visualized in Fig. 2 where ratios of experimentally calculated DDCS to theoretically calculated DDCS have been plotted against the electron energies. A horizontal dashed line has been drawn to indicate the 100% compliance between an experiment and the

theory, below or above which theory overestimates or underestimates the data by a multiplication factor corresponding to *y* axis.

B. Angular distribution of DDCS

Figure 3 shows the angular distributions of DDCS for a few energies along with the CDW-EIS and CTMC calculations. These plots are useful in visualizing the angular asymmetry of the DDCS at particular electron energy. The energies are selected to represent the full energy range of the spectrum. However, energies are not selected near the K-LL Auger electron region since it represents an entirely different ionization mechanism, namely the inner-shell process. The difference in DDCS at extreme forward and backward angles for low-energy electrons is about one order of magnitude and that gradually increases to about two orders of magnitude for high-energy electrons. For example, the e-DDCS, for electron energy around 140–220 eV, at 150 degree is about 40–50 times smaller compared to that at 20 degrees. Since this background contribution (on which the KLL peak rides) goes down drastically in backward angles, the KLL line shows up clearly for large backward angles. This explains why the KLL peak is more clearly visible in backward angles in Fig. 1.

TABLE I. Data table for measured DDCS ($cm^2 eV^{-1} Sr^{-1}$), SDCS, and TCS for water bombarded by 250-keV H^+ projectiles. Numerals in square brackets indicate the power of 10.

E	30°	45°	60°	75°	80°	90°	105°	120°	135°	150°	$(d\sigma/d\epsilon_e)$
1	1.5[−18]	1.0[−18]	1.1[−18]	8.9[−19]	9.0[−19]	8.4[−19]	7.6[−19]	7.6[−19]	8.0[−19]	6.7[−19]	9.6[−18]
5	1.2[−18]	1.0[−18]	9.7[−19]	7.7[−19]	7.2[−19]	6.1[−19]	5.9[−19]	4.9[−19]	4.9[−19]	4.1[−19]	7.7[−18]
9	8.4[−19]	7.3[−19]	6.2[−19]	5.2[−19]	4.6[−19]	3.7[−19]	3.3[−19]	2.6[−19]	2.5[−19]	2.0[−19]	4.8[−18]
11	7.2[−19]	6.2[−19]	5.2[−19]	4.3[−19]	3.7[−19]	3.1[−19]	2.7[−19]	2.0[−19]	1.9[−19]	1.5[−19]	4.1[−18]
15	5.7[−19]	4.9[−19]	4.0[−19]	3.1[−19]	2.7[−19]	2.2[−19]	1.8[−19]	1.3[−19]	1.2[−19]	9.6[−20]	2.9[−18]
19	4.5[−19]	3.8[−19]	3.1[−19]	2.4[−19]	2.1[−19]	1.6[−19]	1.2[−19]	8.2[−20]	8.2[−20]	6.6[−20]	2.2[−18]
25	3.3[−19]	2.9[−19]	2.3[−19]	1.6[−19]	1.4[−19]	1.0[−19]	7.2[−20]	5.1[−20]	4.8[−20]	4.0[−20]	1.7[−18]
35	2.3[−19]	1.9[−19]	1.5[−19]	1.1[−19]	8.9[−20]	6.7[−20]	3.7[−20]	2.6[−20]	2.6[−20]	2.4[−20]	1.1[−18]
60	1.2[−19]	1.0[−19]	7.9[−20]	4.9[−20]	3.9[−20]	2.3[−20]	1.3[−20]	9.5[−21]	9.4[−21]	8.3[−21]	4.5[−19]
100	5.9[−20]	5.2[−20]	3.5[−20]	1.8[−20]	1.2[−20]	6.1[−21]	3.7[−21]	3.1[−21]	3.1[−21]	2.7[−21]	1.9[−19]
140	3.5[−20]	3.0[−20]	1.8[−20]	6.8[−21]	4.5[−21]	2.3[−21]	1.5[−21]	1.3[−21]	1.2[−21]	1.1[−21]	9.5[−20]
180	2.3[−20]	1.9[−20]	9.9[−21]	2.6[−21]	1.7[−21]	1.1[−21]	6.7[−22]	6.0[−22]	5.7[−22]	5.1[−22]	5.4[−20]
220	1.6[−20]	1.3[−20]	4.9[−21]	1.2[−21]	8.7[−22]	5.7[−22]	4.3[−22]	3.6[−22]	3.2[−22]	3.0[−22]	3.3[−20]
260	1.2[−20]	8.1[−21]	2.4[−21]	6.1[−22]	4.6[−22]	2.9[−22]	2.4[−22]	2.0[−22]	1.8[−22]	1.3[−22]	2.1[−20]
300	9.1[−21]	5.2[−21]	1.2[−21]	3.3[−22]	2.4[−22]	1.9[−22]	1.5[−22]	1.3[−22]	1.0[−22]	8.8[−23]	1.3[−20]
340	6.9[−21]	3.2[−21]	5.8[−22]	2.2[−22]	1.7[−22]	1.1[−22]	1.0[−22]	7.7[−23]	6.5[−23]	5.6[−23]	8.5[−21]
380	5.0[−21]	1.8[−21]	3.0[−22]	1.3[−22]	1.0[−22]	7.1[−23]	7.4[−23]	6.6[−23]	4.7[−23]	3.7[−23]	5.4[−21]
420	3.4[−21]	9.9[−22]	2.2[−22]	8.7[−23]	7.4[−23]	6.1[−23]	5.8[−23]	4.3[−23]	3.9[−23]	3.1[−23]	3.4[−21]
460	2.3[−21]	5.7[−22]	1.5[−22]	9.8[−23]	9.0[−23]	7.7[−23]	7.8[−23]	7.0[−23]	6.5[−23]	5.2[−23]	2.5[−21]
480	1.8[−21]	4.4[−22]	1.6[−22]	1.1[−22]	1.1[−22]	9.5[−23]	1.1[−22]	1.0[−22]	9.2[−23]	8.0[−23]	2.3[−21]
500	1.4[−21]	3.6[−22]	1.1[−22]	9.3[−23]	8.9[−23]	8.0[−23]	9.6[−23]	9.3[−23]	7.3[−23]	6.5[−23]	1.7[−21]
510	1.2[−21]	2.9[−22]	8.5[−23]	7.1[−23]	6.9[−23]	7.0[−23]	6.6[−23]	6.2[−23]	5.2[−23]	4.5[−23]	1.4[−21]
530	9.4[−22]	1.8[−22]	5.9[−23]	3.7[−23]	3.6[−23]	3.7[−23]	3.1[−23]	2.4[−23]	1.4[−23]	1.4[−23]	1.0[−21]
560	5.9[−22]	1.2[−22]	4.7[−23]	2.5[−23]	2.5[−23]	3.6[−23]	2.6[−23]	1.6[−23]	3.1[−23]	9.5[−24]	6.5[−22]
600	3.2[−22]	7.0[−23]	3.3[−23]	1.9[−23]	1.8[−23]	2.0[−23]	2.2[−23]	1.3[−23]	8.9[−24]	7.4[−24]	3.9[−22]
$(d\sigma/d\Omega_e)$	3.4[−17]	2.9[−17]	2.3[−17]	1.6[−17]	1.4[−17]	1.1[−17]	9.1[−18]	7.3[−18]	7.2[−18]	6.0[−18]	1.6[−16] (TCS)

The forward-backward angular asymmetry in e-DDCS is explained in Sec. V C. The CDW-EIS theory overestimates the experimental data within the energy range of 1–40 eV for all angles. For higher energies and forward angles, CDW-EIS calculations qualitatively match with the experimental data but in the backward angles it underestimates the experimental data. This underestimation, for large enough emission energies, is considerably reduced by taking into account the $\tilde{Z}_{eff}(\theta)$ effective charge. Interestingly, the angular distribution of DDCS calculated by the CTMC model shows excellent agreement with the experimental data within 80–400 eV. For lower energies, CTMC shows small deviations from the experimental data for almost all angles, an expected behavior given the inherent problem of CTMC with the soft collision process.

C. Asymmetry parameter

The importance of studying forward-backward angular asymmetry is to understand the electron angular distribution, which varies due to its postcollisional interaction with the projectile ions. It has been studied through the forward-backward asymmetry parameter (FBAP) calculated using the following formula [34];

$$\alpha(\epsilon_e, \theta) = \frac{\sigma(\epsilon_e, \theta) - \sigma(\epsilon_e, \pi - \theta)}{\sigma(\epsilon_e, \theta) + \sigma(\epsilon_e, \pi - \theta)}, \qquad (2)$$

where, $\sigma(\epsilon_e, \theta)$ and $\sigma(\epsilon_e, \pi - \theta)$ denote the absolute DDCS at the lowest forward angle (θ) and its exact opposite back-

ward angle $(\pi - \theta)$. Since the angular distribution of DDCS (Fig. 3) vary slowly at 30° and 150°, we have calculated the FBAP at these complementary angles. Experimentally calculated FBAP and results from CTMC, CDW-EIS, and, DC-CDW-EIS models have been plotted against the emitted electron energy as shown in Fig. 4. The asymmetry in electron emission in opposite angles arises partially from the two center effect due to the superposition of the fields of the residual target and the projectile nucleus. It has been shown that it is also partly due to the non-Coulomb potential of the many-electron systems. The gradual increase in the FBAP is due to the gradually decreasing impact parameter and therefore increasing two center influence, which is well reflected by the CDW-EIS model that includes the above mechanisms. The experimentally calculated FBAP matches well with the CDW-EIS model as compared to the CTMC calculations. The CTMC calculations give excellent agreement within 20–400 eV whereas the CDW-EIS model matches well in low- and high-energy regions except for 40–200 eV. The results obtained from DC-CDW-EIS calculations in high emission energies are better than CDW-EIS calculations and comparable to the CTMC predictions.

D. Single differential cross section

The SDCS values were obtained for all angles by numerically integrating the DDCS data, $d^2\sigma/d\epsilon_e d\Omega_e$, over energy, i.e., $(d\sigma/d\Omega_e)$ and over emission angles, i.e., $(d\sigma/d\epsilon_e)$. The
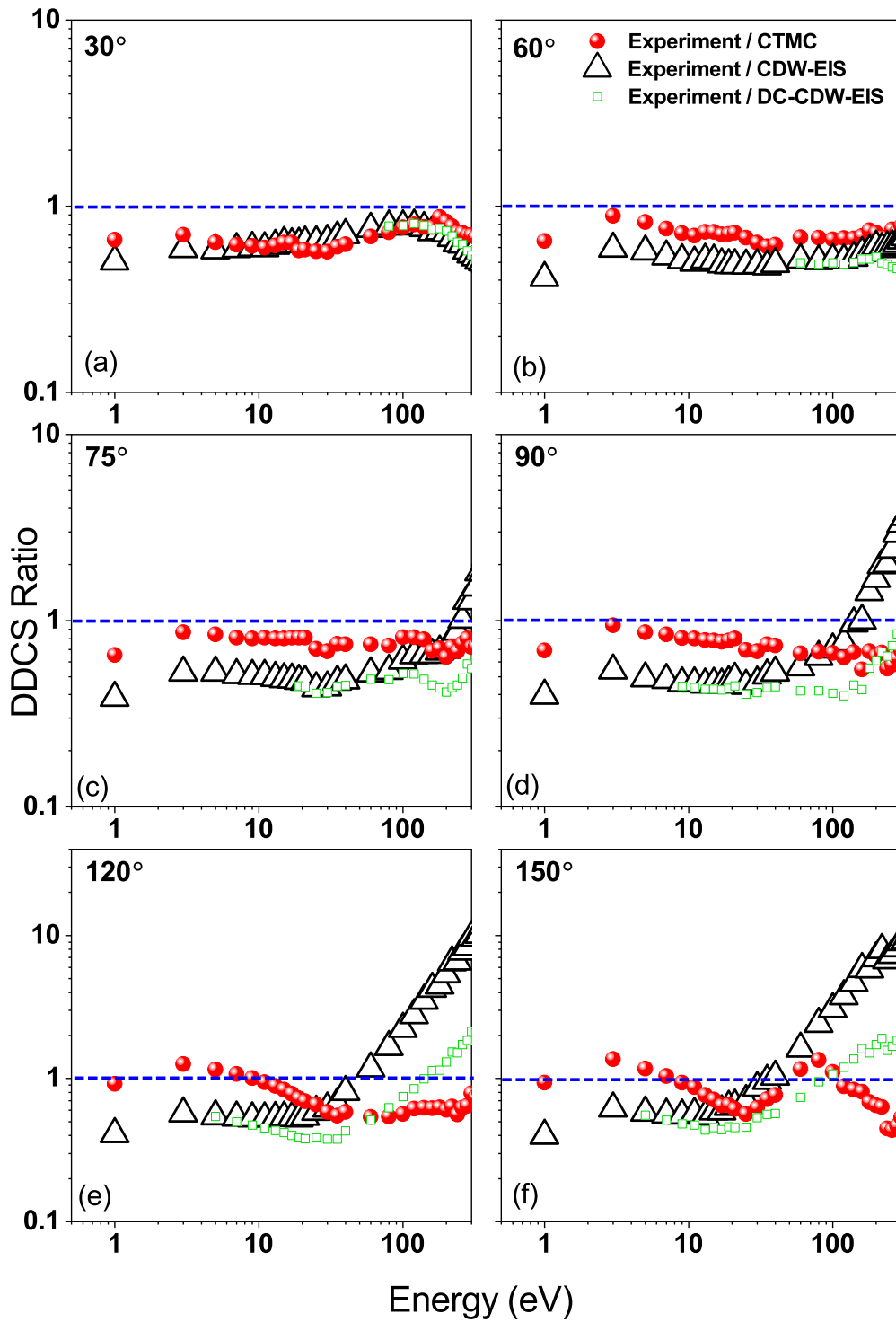
FIG. 2. Ratio of the measured DDCS to theoretically calculated DDCS for six angles.

integrations have been performed over the electron energy range of 1–600 eV and angles from 30–150 degrees to get energy distribution and angular distribution of the SDCS as shown in Figs. 5(a) and 5(b). The comparison between theoretical and experimental SDCS has been shown by plotting their ratios (i.e., experiment divided by theory) in Figs. 5(c) and 5(d). It is observed that the energy distribution of SDCS calculated by the CDW-EIS model is about 1.5–2.5 times the

experimental data and interestingly the CTMC model provides a much improved agreement, which is about 1–1.5 times the experimental data, except at high energy. The sudden variation at 480 eV in Fig. 5(c) is due to the presence of the Auger electron emission peak in experimental DDCS. The angular distribution of SDCS by the CTMC model gives excellent compliance with the experimental SDCS as compared with the CDW-EIS model.
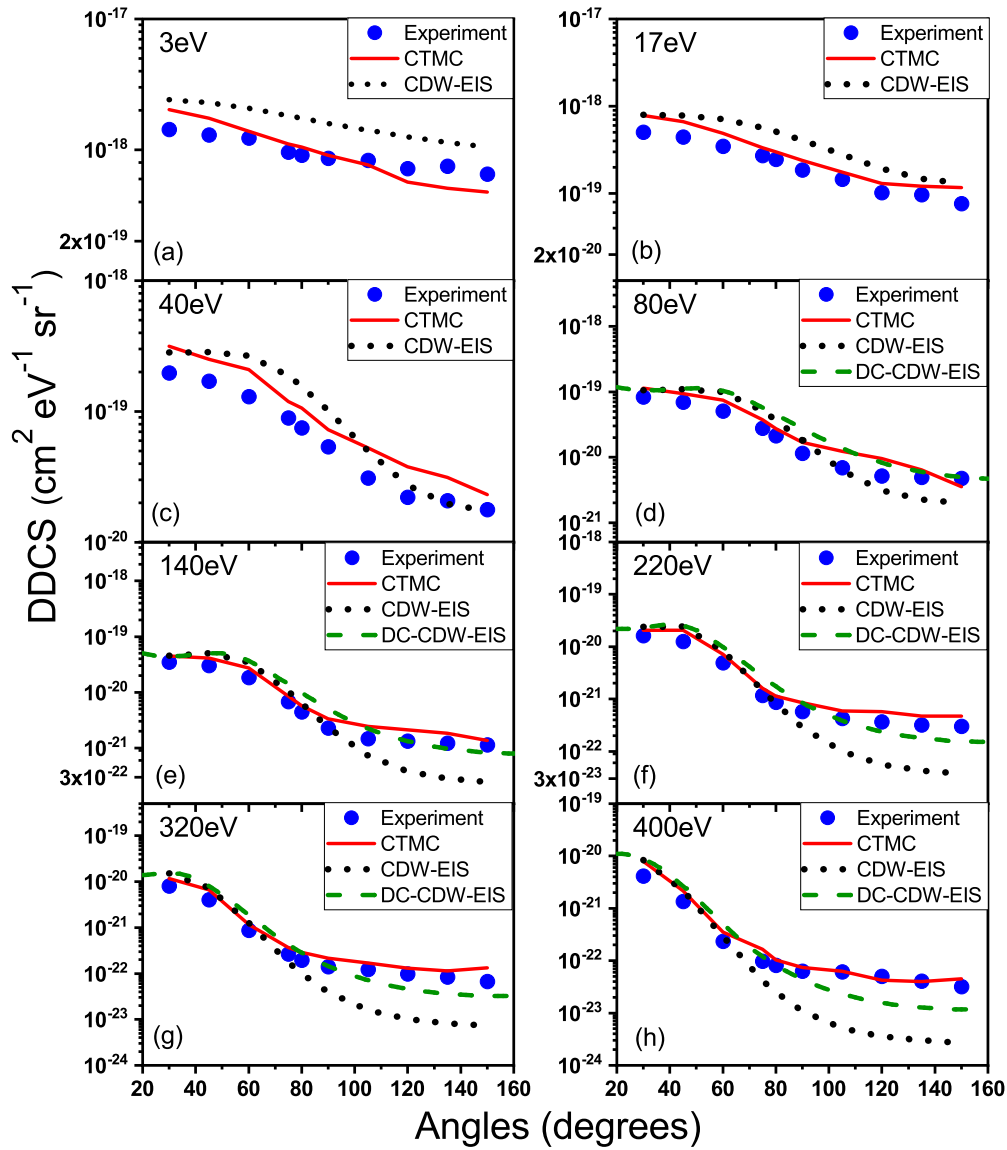
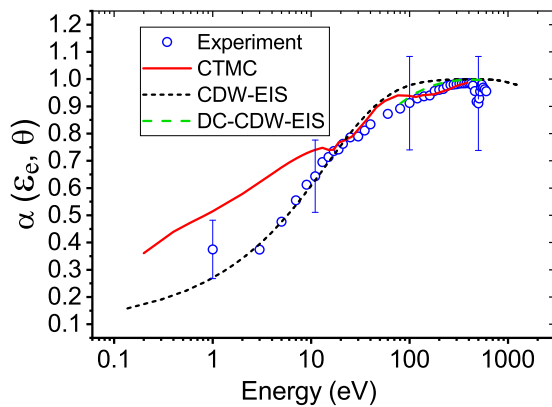FIG. 3. Angular distribution of DDCS at few energies along with the CTMC, CDW-EIS, and DC-CDW-EIS calculations.

E. Estimation of total cross section (TCS)

The TCSs have been obtained by integrating the experimental as well as theoretical SDCS values over 0–180°. The linear extrapolation of SDCS was carried at extreme lower and higher angles. From Table II, it is clearly seen that TCS for water obtained from the experiment matches well with the CTMC calculations as compared to the CDW-EIS calculations. Both the theories overestimated the experimentally calculated values and lie within the same order of magnitude.

FIG. 4. Forward-backward asymmetry parameter versus electron energy calculated using angles $\theta = 30°$ and $\theta = 150°$.

TABLE II. TCS values for water target for 250-keV H^+ projectiles.

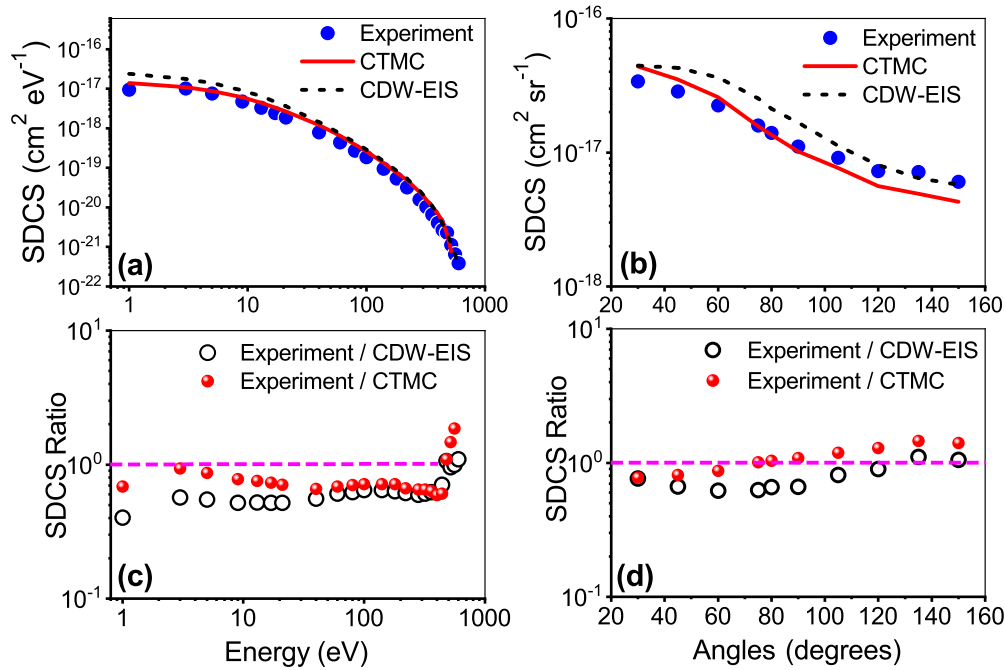|	Total cross section (cm^2)
Experimental	1.62×10^{-16}
CDW-EIS model	2.99×10^{-16}
CTMC model	2.14×10^{-16}

FIG. 5. (a) Energy distribution and (b) angular distribution of absolute SDCS. (c) and (d) represent ratio of experimental-to-theoretical SDCS for (a) and (b), respectively.

However the CTMC approach provides a much better agreement with the experiment with deviation about 30%.

VI. CONCLUSIONS

We have studied the interaction of 250-keV proton with neutral H_2O molecules by measuring the emitted electron energy distribution for ten different emission angles within $30°$ and $150°$. The obtained DDCS, SDCS, and TCS have been compared with three state-of-the-art different models, i.e., CDW-EIS and recently upgraded DC-CDW-EIS and CTMC models. The new calculations of CTMC includes the influence of time-dependent dynamic screening. Experimentally measured absolute DDCS shows excellent agreement with the CTMC calculations whereas the CDW-EIS gave qualitative agreement in forward angles. The forward-backward angular asymmetry increases with the increase in electron energy, which is due to the influence of two-center effect. Both models show a comparatively better match with the experimentally estimated FBAP at high electron energies. However, below 10 eV, the CTMC model diverged from the experimental data. The energy distribution and angular distribution of SDCS calculated by CTMC theory gives an excellent match with the experimental results as compared to that with the CDW-EIS model calculations. Experimental TCS matches well with that calculated by the CTMC model (which overestimates by 32%) whereas, the CDW-EIS model provided 84% overestimation

compared to the experimental ones. The present data provides a stringent test of both models, particularly the newly developed CTMC model, which includes time-dependent screening effects.

The use of a dynamic charge in the residual target continuum depending on the emission angle within the CDW-EIS theory (i.e., DC-CDW-EIS) is shown to give a major improvement for backward emission for large enough emission energies. In order to calculate SDCS and TCS the dependence of the dynamic charge with the emission energy should be studied. This a matter for upcoming research. The present set of experimental data on the DDCS of water molecule under relatively low-energy (250-keV) collisions provided a stringent test to the validity of these newly developed state-of-the-art models. It is, however, important to test these models with experimental data over a wider energy range and such experiments are in progress.

[1] F. Gobet, S. Eden, B. Coupier, J. Tabet, B. Farizon, M. Farizon, M. J. Gaillard, M. Carré, S. Ouaskit, T. D. Märk, and P. Scheier, Ionization of water by (20–150)-keV protons: Separation of direct-ionization and electron-capture processes, Phys. Rev. A **70**, 062716 (2004).

[2] E. Scifoni, E. Surdutovich, and A. V. Solov'yov, Spectra of secondary electrons generated in water by energetic ions, Phys. Rev. E **81**, 021903 (2010).

[3] F. A. Cucinotta and M. Durante, Cancer risk from exposure to galactic cosmic rays: implications for space exploration by human beings, Lancet Onc. **7**, 431 (2006).

[4] M. Bernal and J. Liendo, Inelastic-collision cross sections for the interactions of totally stripped H, He and C ions with liquid water, Nucl. Instrum. Meth. Phys. Res. B **262**, 1 (2007).

[5] L. Toburen and W. Wilson, Energy and angular distributions of electrons ejected from water vapor by 0.3–1.5 MeV protons, J. Chem. Phys. **66**, 5202 (1977).

[6] F. Gobet, S. Eden, B. Coupier, J. Tabet, B. Farizon, M. Farizon, M. Gaillard, S. Ouaskit, M. Carré, and T. Märk, Electron-loss and target ionization cross sections for water vapor by 20–150 keV neutral atomic hydrogen impact, Chem. Phys. Lett. **421**, 68 (2006).

[7] M. A. Bolorizadeh and M. E. Rudd, Angular and energy dependence of cross sections for ejection of electrons from water vapor. III. 20–150-keV neutral-hydrogen impact, Phys. Rev. A **33**, 893 (1986).

[8] S. T. S. Kovács, P. Herczku, Z. Juhász, L. Sarkadi, L. Gulyás, and B. Sulik, Ionization of small molecules induced by H$^+$, He$^+$, and N$^+$ projectiles: Comparison of experiment with quantum and classical calculations, Phys. Rev. A **94**, 012704 (2016).

[9] L. Toburen, W. Wilson, and R. Popowich, Secondary electron emission from ionization of water vapor by 0.3 to 2.0 MeV He$^+$ and He^{2+} ions, Radiat. Res. **82**, 27 (1980).

[10] S. Bhattacharjee, S. Biswas, J. M. Monti, R. D. Rivarola, and L. C. Tribedi, Double-differential cross section for ionization of H$_2$O molecules by 4-MeV/u C^{6+} and Si^{13+} ions, Phys. Rev. A **96**, 052707 (2017).

[11] G. Olivera, A. Martinez, R. Rivarola, and P. Fainstein, Theoretical calculation of electronic stopping power of water vapor by proton impact, Radiat. Res. **144**, 241 (1995).

[12] J. Miller and A. Green, Proton energy degradation in water vapor, Radiat. Res. **54**, 343 (1973).

[13] S. Uehara, L. Toburen, W. Wilson, D. Goodhead, and H. Nikjoo, Calculations of electronic stopping cross sections for low-energy protons in water, Radiat. Phys. Chem. **59**, 1 (2000).

[14] C. Mitterschiffthaler and P. Bauer, Stopping cross section of water vapor for hydrogen ions, Nucl. Instrum. Meth. Phys. Res. B **48**, 58 (1990).

[15] M. Shimizu, M. Kaneda, T. Hayakawa, H. Tsuchida, and A. Itoh, Stopping cross sections of liquid water for MeV energy protons, Nucl. Instrum. Meth. Phys. Res. B **267**, 2667 (2009).

[16] C. Tachino, J. Monti, O. Fojón, C. Champion, and R. Rivarola, Ionization of water molecules by ion beams. On the relevance of dynamic screening and the influence of the description of the initial state, J. Phys. B: At. Mol. Opt. Phys. **47**, 035203 (2014).

[17] S. Bhattacharjee, C. Bagdia, M. R. Chowdhury, J. M. Monti, R. D. Rivarola, and L. C. Tribedi, Energy and angular distribution of electrons ejected from water by the impact of fast O^{8+} ion beams, Eur. Phys. J. D **72**, 15 (2018).

[18] A. Jorge, M. Horbatsch, C. Illescas, and T. Kirchner, Classical-trajectory monte carlo calculations of differential electron-emission cross sections in fast heavy-ion collisions with water molecules, Phys. Rev. A **99**, 062701 (2019).

[19] A. Jorge, M. Horbatsch, and T. Kirchner, Multicharged-ion–water-molecule collisions in a classical-trajectory time-dependent mean-field theory, Phys. Rev. A **102**, 012808 (2020).

[20] S. Bhattacharjee, S. Biswas, C. Bagdia, M. Roychowdhury, S. Nandi, D. Misra, J. M. Monti, C. A. Tachino, R. D. Rivarola, C. Champion, and L. C. Tribedi, Double differential distribution of electron emission in the ionization of water molecules by fast bare oxygen ions, J. Phys. B: At. Mol. Opt. Phys. **49**, 065202 (2016).

[21] C. Illescas, L. F. Errea, L. Méndez, B. Pons, I. Rabadán, and A. Riera, Classical treatment of ion-H$_2$O collisions with a three-center model potential, Phys. Rev. A **83**, 052704 (2011).

[22] L. F. Errea, C. Illescas, L. Méndez, and I. Rabadán, Ionization of water molecules by proton impact: Two nonperturbative studies of the electron-emission spectra, Phys. Rev. A **87**, 032709 (2013).

[23] P. Fainstein, V. H. Ponce, and R. D. Rivarola, A theoretical model for ionisation in ion-atom collisions. Application for the impact of multicharged projectiles on helium, J. Phys. B: At. Mol. Opt. Phys. **21**, 287 (1988).

[24] E. Clementi and C. Roetti, Roothaan-Hartree-Fock atomic wavefunctions: Basis functions and their coefficients for ground and certain excited states of neutral and ionized atoms, Z ⩽ 54, At. Data Nucl. Data Tables **14**, 177 (1974).

[25] M. R. Chowdhury and L. C. Tribedi, Electron impact ionization of O$_2$ and the interference effect from forward–backward asymmetry, J. Phys. B: At. Mol. Opt. Phys. **50**, 155201 (2017).

[26] D. Misra, K. Thulasiram, W. Fernandes, A. H. Kelkar, U. Kadhane, A. Kumar, Y. Singh, L. Gulyas, and L. C. Tribedi, Double differential distributions of electron emission in ion–atom and electron–atom collisions using an electron spectrometer, Nucl. Instrum. Meth. Phys. Res. B **267**, 157 (2009).

[27] J. A. Pople, D. P. Santry, and G. A. Segal, Approximate self-consistent molecular orbital theory. I. Invariant procedures, J. Chem. Phys. **43**, S129 (1965).

[28] J. A. Pople and G. A. Segal, Approximate self-consistent molecular orbital theory. II. Calculations with complete neglect of differential overlap, J. Chem. Phys. **43**, S136 (1965).

[29] J. A. Pople and G. A. Segal, Approximate self-consistent molecular orbital theory. III. CNDO results for AB$_2$ and AB$_3$ systems, J. Chem. Phys. **44**, 3289 (1966).

[30] B. Senger and R. V. Rechenmann, Angular and energy distributions of delta-rays ejected from low-z molecular targets by incident protons and alpha particles, Nucl. Instrum. Meth. Phys. Res. B **2**, 204 (1984).

[31] D. Belkić, R. Gayet, and A. Salin, Electron capture in high-energy ion-atom collisions, Phys. Rep. **56**, 279 (1979).

[32] J. M. Monti, O. A. Fojón, J. Hanssen, and R. D. Rivarola, Influence of the dynamic screening on single-electron ionization of multi-electron atoms, J. Phys. B: At. Mol. Opt. Phys. **43**, 205203 (2010).

[33] M. F. Rojas, M. A. Quinto, R. D. Rivarola, and J. M. Monti, Dynamic effective charge in the target continuum within the CDW-EIS model for ionisation in ion-atom collisions: angular dependence, Eur. Phys. J. D **75**, 154 (2021).

[34] R. Nascimento, L. Machado, A. Medina, C. Bielschowsky, and G. Jalbert, The dependence of the forward-backward asymmetry parameter on the molecular orientation in angular distributions of emitted electrons in the rmH_2 ionisation induced by bare ion impact, Eur. Phys. J. D **66**, 225 (2012).